Contrib Mineral Petrol (2001) 141: 287–296
DOI 10.1007/s004100100244

C.A. McCammon · W.L. Griffin · S.R. Shee
H.S.C. O'Neill

Oxidation during metasomatism in ultramafic xenoliths from the Wesselton kimberlite, South Africa: implications for the survival of diamond

Received: 15 August 2000 / Accepted: 16 January 2001 / Published online: 11 April 2001
© Springer-Verlag 2001

Abstract Garnets in xenoliths from the Wesselton kimberlite show significant zoning in major and trace elements. The garnets were studied using room temperature Mössbauer spectroscopy with high spatial resolution, and show an increase in $Fe^{3+}/\Sigma Fe$ from core to secondary rim. Temperatures and pressures were determined using the garnet–olivine, garnet–orthopyroxene and Ni in garnet formulations, and indicate conditions close to 1,000 °C and 37 kbar for most of the garnets. Oxygen fugacities calculated using the garnet–olivine–orthopyroxene oxybarometer show an increase of approximately one log-bar unit from garnet core to secondary rim, relative to the quartz–fayalite–magnetite buffer curve. Combined with reanalysis of literature data from unaltered material from the same locality, there was an increase in relative oxygen fugacity of approximately two log-bar units during the course of metasomatism. Existing data from other South African garnet peridotites were recalculated using the same thermobarometers and oxybarometers, and indicate relative oxygen fugacities that lie at least two log-bar units below the diamond–carbonate equilibrium in peridotitic systems, which defines the maximum limit of diamond stability in peridotite. Diamond would hence be preserved during the initial stages of metasomatism, but in later stages fluid would react with the diamonds, leading to their resorption and eventual destruction.

C.A. McCammon (✉)
Bayerisches Geoinstitut, Universität Bayreuth,
95440 Bayreuth, Germany

W.L. Griffin
Key Centre for Geochemical Evolution
and Metallogeny of Continents,
School of Earth Sciences,
Macquarie University,
Sydney NSW 2109, Australia

S.R. Shee
De Beers Australia Exploration Limited,
Box 126, South Yarra VIC 3141, Australia

H.S.C. O'Neill
Research School of Earth Sciences,
Australian National University,
Canberra ACT 0200, Australia

Editorial responsibility: J. Hoefs

Introduction

The study of zoning profiles in minerals can provide information regarding chemical processes that occurred during the formation of a mineral assemblage. The electron, proton and ion microprobes provide information on major and trace element chemical compositions, but, except in a small number of cases, provide no information on iron oxidation state (e.g. Canil and O'Neill 1996; McCammon 1999; Sobolev et al. 1999). Such information can be used in conjunction with oxygen barometers to determine oxygen fugacity during mineral formation, which can have significant effects on many processes including element partitioning, diffusivity, partial melting reactions and diamond stability. Mössbauer spectroscopy is an excellent method to distinguish between Fe^{2+} and Fe^{3+}, and can provide an estimate of their relative abundance in individual phases. Normally, experiments are performed on polycrystalline samples of ~1 cm diameter, but a simple technique (McCammon et al. 1991; McCammon 1994) enables routine Mössbauer measurements to be performed on absorbers more than two orders of magnitude smaller.

Zoned garnets from phlogopite–harzburgite xenoliths in the Wesselton kimberlite, Kimberly, South Africa, were studied by Griffin et al. (1999) using electron and proton microprobes, and the data were used to infer the history of a multistage metasomatic alteration. Modelling of zoning profiles suggested a three-part process involving infiltration of fluids with different compositions over several different time-scales:

1. Slow diffusion of Ca, Zr and Y from rim to core over periods of 10–30,000 years, from a fluid depleted in Ti, Ga and Y.

2. Formation of garnet overgrowths high in Ca, Zr, Y and Ti, followed by annealing over periods of $\sim 10^3$ years.
3. Formation of secondary rims on very short timescales prior to eruption.

Preliminary work suggested differences in Fe^{3+} concentration between the various garnet generations (McCammon et al. 1995), implying a change in oxygen fugacity conditions.

In this paper we extend the work described by McCammon et al. (1995) and report results of a Mössbauer study of zoned garnets from the Wesselton kimberlite, and calculate oxygen fugacity using the garnet–olivine–orthopyroxene oxybarometer (Luth et al. 1990; Gudmundsson and Wood 1995). Results are used to infer redox conditions during the different processes recorded in the zoning patterns and their implications for diamond stability.

Experimental procedure

Mineral fragments from ultramafic xenoliths in coarse concentrate from the Wesselton kimberlite were mounted in epoxy disks and polished for preliminary analysis using the electron and proton microprobes. Garnets showing significant heterogeneity were prepared as polished sections to determine zoning patterns using the electron microprobe at CSIRO and Macquarie University (Australia) and the proton microprobe at CSIRO (Australia). Coexisting olivine and orthopyroxene were found to be homogeneous within each grain. X-ray maps of the garnets were prepared and used to locate interesting areas for Mössbauer analysis. Descriptions of the four garnets selected for this study are listed in Table 1, and chemical compositions are listed in Griffin et al. (1999).

Samples were prepared for Mössbauer spectroscopy by grinding the disks to a thickness of $\sim$300 μm, which gives an iron density of $\sim$5 mg Fe/cm^2 based on the chemical composition of the garnet. Note that because Mössbauer spectroscopy is a non-destructive technique, the top polished surface of the disks are preserved for further analysis. To isolate different parts of the sample, a piece of 25-μm thick Ta foil (absorbs 99.9% of 14.4 keV gamma rays) drilled with a 400-μm diameter hole was positioned over the area to be analysed. Ca X-ray maps showing the locations where Mössbauer spectra were collected are illustrated in Fig. 1.

A simple modification to a conventional Mössbauer spectrometer allows spectra of absorbers nearly two orders of magnitude smaller diameter to be collected (McCammon et al. 1991; McCammon 1994). To obtain adequate count rates, a conventional Mössbauer source (typical specific activity 100 mCi/cm^2) is replaced by a point source (specific activity ≥2,000 mCi/cm^2), which can be obtained commercially at a cost similar to conventional sources. The gamma rays are collimated to the selected absorber diameter using a Pb shield, and the source-absorber distance is reduced to < 5 mm. The latter results in a solid angle similar to conventional experiments, and hence a similar count rate. Because the signal quality depends on absorber density (measured in mg Fe/cm^2) and not the total amount of iron in the absorber, the reduction in size has no effect on the effective thickness of the absorber. When non-resonant absorption caused by heavier elements is low and the point source is relatively new (< 1 year old), high quality Mössbauer spectra (comparable to conventional measurements) can be recorded on absorbers with diameters as small as 50 μm.

Mössbauer spectra were recorded at room temperature in transmission mode using a constant acceleration Mössbauer spectrometer with a nominal 20 mCi ^{57}Co high specific activity source (2 Ci/cm^2) in a 12-μm Rh matrix. Spectra were collected over time periods ranging from 1–5 days, depending on the signal quality. The velocity scale was calibrated relative to 25 μm α-Fe foil using the positions certified for National Bureau of Standards standard reference material no. 1541; line widths of 0.42 mm/s for the outer lines of α-Fe were obtained at room temperature. The spectra were fitted to Lorentzian and Voigt line-shapes using the commercially available fitting program NORMOS written by R.A. Brand (distributed by Wissenschaftliche Elektronik GmbH, Germany).

Results from Mössbauer spectroscopy

The Mössbauer spectra of garnet were fitted to two quadrupole doublets, corresponding to Fe^{2+} and Fe^{3+}. Spectra were initially fit to Lorentzian doublets with conventional constraints (equal component widths and areas), but residuals showed large deviations. Final fits were therefore obtained using Voigt doublets for Fe^{2+} absorption, where areas and Lorentzian line-widths of individual components were allowed to vary, and Lorentzian doublets with conventional constraints for Fe^{3+} absorption. Area asymmetry reflects recoil-free fraction anisotropy (Gol'danskii–Karyagin effect; Geiger et al. 1992), whereas line-width asymmetry probably reflects differences in next-nearest neighbour configurations (e.g. Angel et al. 1998). Although line-width and area asymmetry parameters are correlated and cannot be determined unambiguously, the high resolution of Fe^{2+} and Fe^{3+} absorption enables robust values for other hyperfine parameters (centre shift, quadrupole splitting and relative area) to be determined.

Hyperfine parameters for Fe^{2+} (Table 2) correspond to those reported by Amthauer et al. (1976) for the

Table 1 Description of zoned garnets studied using Mössbauer spectroscopy

Sample	Description
933	A single grain ~1.6×2.5 mm, surrounded by olivine and orthopyroxene. Composition varies somewhat irregularly from core to rim, and the grain is surrounded by a secondary garnet rim that varies from 100–150 μm in thickness
937	A single ovoid grain, of which an area ~1.7 mm across is available for analysis. It is surrounded by olivine. There is pronounced zoning from core to rim, and a secondary replacement rim of up to 500 μm in thickness
940	A single grain ~3.5 mm in the long diameter, surrounded by olivine and orthopyroxene. The primary garnet grain shows broad symmetrical zoning from core to rim, and on one side there is a 50–75 μm zone of secondary replacement garnet
951	An incomplete grain ~3 mm in diameter, surrounded by olivine and orthopyroxene. The relatively homogeneous core is surrounded by a rim of distinctly different composition

dodecahedral site, and agree within experimental error with values reported by Luth et al. (1990) for mantle-derived garnets of similar composition. Hyperfine parameters of Fe^{3+} correspond to those reported in the above references for the octahedral site, and there is no evidence for tetrahedrally coordinated Fe^{3+}. Line-widths for both Fe^{2+} and Fe^{3+} doublets are somewhat greater than values commonly observed for mantle garnets, which is likely related to microstresses in the single crystals and would normally be removed during grinding. The increased line-widths do not have a significant effect on the values determined for $Fe^{3+}/\Sigma Fe$.

Fe^{3+} contributions are well resolved in all spectra consisting primarily of garnet, and relative areas could be determined with high precision. De Grave and Van Alboom (1991) have shown that recoil-free fractions of sites containing Fe^{3+} tend to be larger than for sites containing Fe^{2+}, which agrees with observations for garnet (e.g. Lyubutin et al.1970; Lyubutin and Dodokin 1971; Amthauer et al. 1976). Accordingly, we corrected the relative areas of Fe^{3+} components to determine $Fe^{3+}/\Sigma Fe$ as described by Rancourt et al. (1994) using values for the Mössbauer Debye temperatures of $\Theta_M(Fe^{2+}) = 340$ K and $\Theta_M(Fe^{3+}) = 500$ K, which are similar to values reported by De Grave and Van Alboom (1991) for other silicates. We did not correct the relative areas for thickness effects because these are minimal considering the large intrinsic line-widths combined with the small effective thicknesses of the garnets (e.g. Rancourt et al. 1993). $Fe^{3+}/\Sigma Fe$ values vary in a consistent manner in all garnets studied, where values increase from core to secondary rim (Table 2). Figure 2 illustrates Mössbauer spectra taken from different regions of the garnets.

We collected Mössbauer spectra for minerals coexisting with garnet (Fig. 3). Mössbauer spectra for olivine give hyperfine values that agree with those in the literature (e.g. Shinno 1981) and show no evidence for Fe^{3+} within the detection limit (~2% $Fe^{3+}/\Sigma Fe$). Mössbauer spectra for orthopyroxene show unequal component areas because of preferred orientation (the absorbers are single crystals) and the non-cubic point group symmetry of the iron sites. Hyperfine parameters indicate that most Fe^{2+} is partitioned into the M2 site, and values are consistent with those observed for other mantle orthopyroxenes of similar composition (e.g. Luth and Canil 1993). Values for $Fe^{3+}/\Sigma Fe$ in olivine and orthopyroxene are consistent with results from other Mössbauer studies of mantle xenoliths (e.g. Canil and O'Neill 1996).

Several spectra collected from garnet rims showed additional absorption (Fig. 3, bottom), and compari-

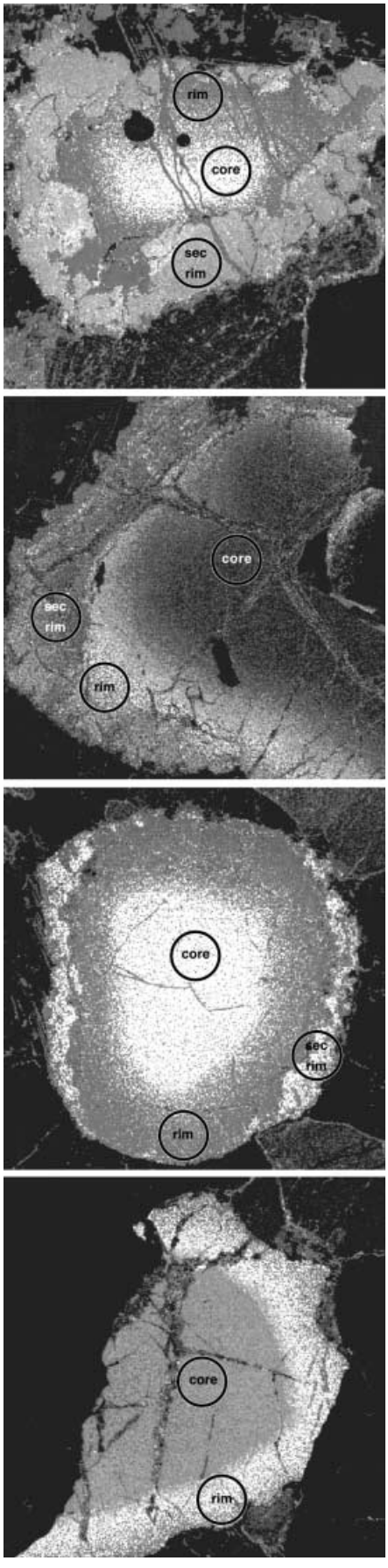

Fig. 1 Electron microprobe X-ray maps of garnet grains indicating distribution of Ca (data from Griffin et al. 1999). Samples are ordered in the sequence (top to bottom): 933; 937; 940; 951. Transmission Mössbauer spectra were recorded of the regions marked by *circles* (400 μm diameter), where labels correspond to those given in Table 2

Table 2 Room temperature hyperfine parameters of garnets and coexisting minerals. *CS* Centre shift (relative to α-Fe); *QS* quadrupole splitting; Γ Lorentzian full width at half maximum of low-velocity component; *σ* Gaussian standard deviation; A_{21} component area asymmetry; Γ_{21} component line-width asymmetry. Estimated standard deviations for garnet spectra are ±0.005 mm/s (CS and QS); ±0.01 mm/s (Γ and *σ*); ±0.05 (A_{21} and Γ_{21}). Estimated standard deviations for opx and ol spectra are ±0.01 mm/s (CS and QS); ±0.01 mm/s (Γ). Parameter values in italics were held fixed during the fitting process

Sample	Fe^{2+}						Fe^{3+}			Phase	
	CS (mm/s)	QS (mm/s)	Γ (mm/s)	*σ* (mm/s)	A_{21}	Γ_{21}	CS (mm/s)	QS (mm/s)	Γ (mm/s)	Relative area (%)	$Fe^{3+}/\Sigma Fe$[a] (%)
Garnet 933											
Core	1.288	3.555	0.36	0.1	0.98	0.87	0.347	0.337	0.31	100	6 (2)
Rim	1.321	3.583	0.48	–	*0.95*	0.81	*0.354*	0.373	*0.45*	55	12 (9)
Sec rim	1.292	3.563	0.32	0.18	0.93	0.79	0.385	0.000	0.61	95	10 (3)
Garnet 937											
Core	1.292	3.557	0.3	0.27	0.95	0.77	*0.354*	0.262	*0.50*	100	5 (2)
Rim	1.284	3.522	0.22	0.27	0.96	0.98	*0.354*	0.365	*0.50*	92	9 (3)
Sec rim	1.316	3.584	0.47	–	*0.95*	0.82	*0.354*	0.346	*0.45*	53	10 (7)
Garnet 940											
Core	1.309	3.606	0.41	0.07	0.96	0.82	0.344	0.247	0.46	100	5 (2)
Rim	1.314	3.585	0.47	0.06	0.89	0.78	0.404	0.265	0.31	98	4 (2)
Sec rim	1.321	3.587	0.46	–	0.95	0.83	*0.354*	0.340	*0.45*	44	7 (6)
Garnet 951											
Core	1.285	3.578	0.39	0.14	0.99	0.82	*0.354*	0.405	0.48	100	5 (2)
Rim	1.300	3.541	0.4	0.15	0.95	0.76	*0.354*	0.000	0.69	91	6 (3)
Coexisting minerals											
Orthopyroxene 933	1.15	2.13	0.45							100	0 (2)
Orthopyroxene 951	1.13	2.13	0.41				0.24	0.82	*0.41*	100	2 (2)
Olivine 937	1.14[b]	2.98[b]	0.41[b]							100	0 (2)

[a]Corrected for differential recoil-free fractions assuming Θ_M (Fe^{2+}) = 340 K; Θ_M (Fe^{3+}) = 500 K
[b]Weighted mean values for all Fe^{2+} absorption

son of hyperfine parameters with literature values suggests the presence of spinel and phlogopite. Griffin et al. (1999) reported grain-boundary replacement of garnet by phlogopite, with inclusions of chrome spinel. This was confirmed in the present samples using an optical microscope. The iron content of the spinel is significantly higher than that of the phlogopite, which is reflected in the relative intensities of Mössbauer absorption. To fit garnet spectra containing these additional phases, we added doublets corresponding to Fe^{2+} and Fe^{3+} in each phase, and constrained hyperfine values (centre shift, quadrupole splitting and line-width) to those reported in the literature for spinel and phlogopite with similar composition (spinel: Osborne et al. 1981; phlogopite: Canil and O'Neill 1996). The larger uncertainties in $Fe^{3+}/\Sigma Fe$ for garnet (Table 2) reflect primarily uncertainties in the assumption of equal component areas for phlogopite. Mössbauer sites in spinel have cubic point group symmetry, hence component areas will be equal even for single crystals (Gibb 1978), but, in the case of phlogopite, component areas vary with orientation. Nevertheless, component areas of phlogopite are relatively well constrained by the high resolution of the Mössbauer spectrum in the relevant velocity range, and appear to be close to 1:1. This is consistent with petrographic observations that phlogopite is fine-grained compared with the garnet, and would imply that there is no significant preferred orientation. In support of our fitting approach, the few garnet spectra that contain absorption from spinel and phlogopite gave $Fe^{3+}/\Sigma Fe$ garnet values that were consistent with results from garnet-only spectra.

Thermobarometry

The garnets in the harzburgitic xenoliths that we studied showed marked chemical zoning over several hundred microns, whereas coexisting olivine and orthopyroxene are homogeneous based on electron microprobe data. Olivine and orthopyroxene dominate the assemblage (62 and 27 vol%, respectively, according to the Wesselton sample studied by Carswell and Dawson 1970), compared with the minor amount of garnet (3 vol%). Because olivine and orthopyroxene account for ~90% of Fe and Mg in the rock and partitioning of Fe^{2+} and Mg between these phases is not significantly temperature dependant, Fe^{2+}/Mg in both phases is not likely to change during metasomatism unless there was a large amount of fluid that was significantly out of equilibrium with regard to Fe^{2+}/Mg.

We therefore assumed that Fe^{2+}/Mg of olivine and orthopyroxene remained constant throughout all stages of metasomatism, whereas the garnet Fe/Mg composition changed in response to the different conditions,

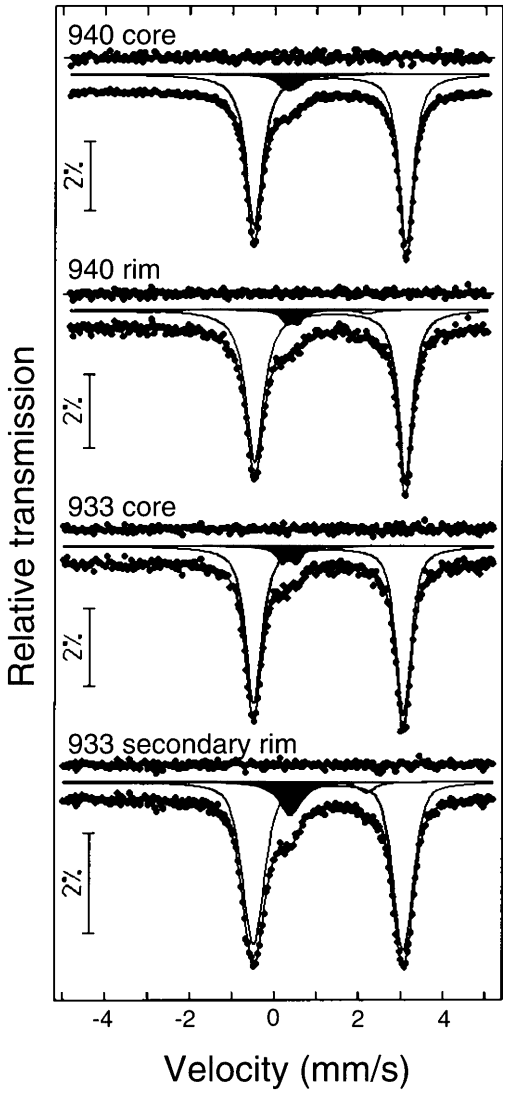

Fig. 2 Room temperature Mössbauer spectra of zoned garnets illustrating the variation in Fe^{3+} absorption (*shaded black*) between core and rim (garnet 940), and core and secondary rim (garnet 933)

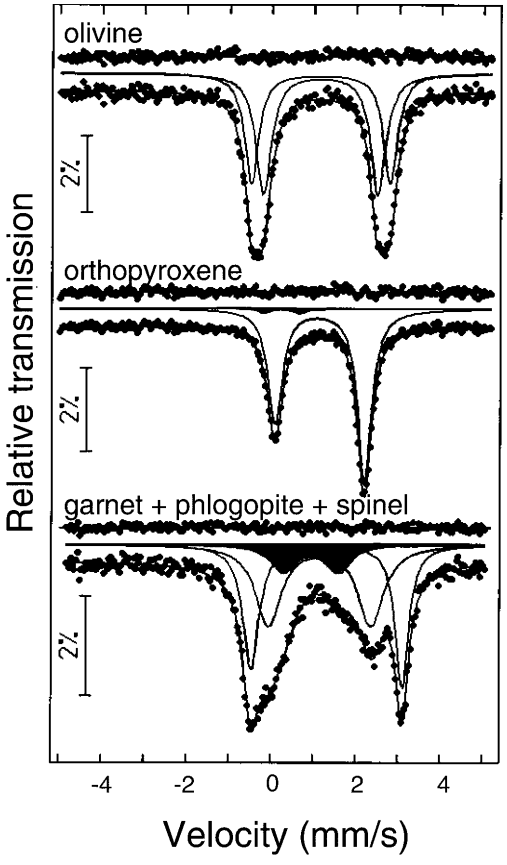

Fig. 3 Room temperature Mössbauer spectra of minerals coexisting with garnet taken from samples 937 (*top*); 951 (*middle*); and 937 (*bottom*). Subspectra are shaded as follows: *black* (Fe^{3+}); *light grey* (Fe^{2+} in phlogopite); *dark grey* (Fe^{2+} in spinel)

allowing temperatures to be estimated based on either the garnet–orthopyroxene or garnet–olivine thermometers. Pressures were estimated from the Al in orthopyroxene (equilibrated with garnet) barometer, but could not be determined for all stages of metasomatism. Hence, we calculated pressures based on the composition of the garnet rims equilibrated with orthopyroxene, and assumed that pressure remained relatively constant throughout the metasomatism. It should be emphasised, however, that all of the above assumptions regarding thermobarometry contribute a relatively minor uncertainty to the determination of oxygen fugacity (see the following section).

The garnet–olivine thermometer of O'Neill and Wood (1979, 1980; OW79) and the garnet–orthopyroxene thermometer of Harley (1984a; H84a) give temperatures that generally agree within $\pm 50°$ of one another (Table 3). All of the garnet cores and rims, as well as one of the secondary rims, show temperatures of approximately 1,000 °C, whereas the other two secondary rims show temperatures approximately 200 °C higher. The Ni-in-garnet thermometer (Griffin et al. 1989; Ryan et al. 1996; G89) provides an independent temperature determination based on the Ni content of garnet, assumed to have equilibrated with olivine. Temperatures from the Ni-in-garnet thermometer are also near 1,000 °C, with two exceptions showing temperatures up to 300 °C higher (Table 3). Similar results are obtained if the Ni-in-garnet thermometer calibration of Canil (1999; C99) is used. Pressures were calculated to be ~37 kbar using the Al in orthopyroxene barometer of Brey and Köhler (1990; BK90), where orthopyroxene was assumed to be in equilibrium with the garnet rims. Similar pressures were obtained using the formulation of Harley (1984b; H84b).

The P,T estimates for the metasomatised garnet harzburgites from the Wesselton kimberlite are consistent with results from other garnet lherzolites and harzburgites from South Africa and neighbouring localities (Table 4 and Fig. 4). We used the analyses reported by Luth et al. (1990) and Canil and O'Neill (1996) to determine P,T conditions according to either (1) the two-pyroxene thermometer of Brey and Köhler

Table 3 Calculated equilibrium conditions and oxygen fugacities of zoned garnet xenoliths from Wesselton kimberlite

	933			937			940			951	
	Core	Rim	Sec rim	Core	Rim	Sec rim	Core	Rim	Sec rim	Core	Rim
Thermobarometry											
T_{gt-ol}(OW79), °C	986	1,022	1,238	951	1,000	1,161	935	968	998	990	957
+ P_{gt-opx}(BK90), kbar		37.3			37.5			36.6			35.3
T_{gt-opx}(H84a), °C	998	1,005	1,113	997	987	1,080	961	964	998	976	932
+ P_{gt-opx}(H84b), kbar		38.1			37.5			38.2			34.5
T_{Ni}(G89), °C	1,025	1,233	1,012	1,038	1,018	1,305	971	992	1,025	985	985
T_{Ni}(C99), °C	1,063	1,188	1,055	1,075	1,063	1,233	1,027	1,041	1,062	1,039	1,039
P used, kbar	37.3	37.3	37.3	37.5	37.5	37.5	36.6	36.6	36.6	35.3	35.3
T used, °C	986	1,022	1,238	951	1,000	1,161	935	968	998	990	957
Olivine/orthopyroxene compositions											
x_{Fa}	0.069	0.069	0.069	0.063	0.063	0.063	0.059	0.059	0.059	0.058	0.058
x_{Fs}	0.061	0.061	0.061	0.056	0.056	0.056	0.052	0.052	0.052	0.050	0.050
Cations in garnet (based on 12 O)											
Si	2.991	2.977	3.018	3.001	3.027	2.981	2.979	2.970	3.004	3.026	3.023
Ti	0.016	0.022	0.031	0.005	0.019	0.028	0.002	0.010	0.009	0.001	0.021
Al	1.521	1.526	1.538	1.551	1.568	1.524	1.492	1.520	1.546	1.605	1.599
Cr	0.444	0.449	0.396	0.425	0.371	0.403	0.481	0.441	0.398	0.380	0.338
Fe^{2+}	0.353	0.321	0.298	0.337	0.308	0.292	0.326	0.322	0.305	0.293	0.303
Fe^{3+}	0.021	0.044	0.031	0.016	0.030	0.031	0.019	0.016	0.022	0.017	0.018
Mn	0.021	0.021	0.014	0.016	0.018	0.010	0.009	0.019	0.013	0.017	0.015
Ni	0.000	0.000	0.000	0.000	0.000	0.001	0.000	0.000	0.000	0.000	0.000
Mg	2.341	2.272	2.443	2.512	2.282	2.538	2.457	2.376	2.427	2.474	2.306
Ca	0.297	0.376	0.213	0.138	0.357	0.219	0.267	0.361	0.288	0.165	0.360
Na	0.008	0.015	0.001	0.008	0.007	0.004	0.003	0.010	0.004	0.004	0.012
Oxygen fugacity											
log f_{O_2}(FMQ), bar	–2.2(5)	–1.2(10)	–1.6(4)	–2.4(6)	–1.5(5)	–1.4(9)	–1.9(5)	–2.3(7)	–1.7(11)	–1.9(5)	–1.9(7)

Table 4 Oxygen fugacities of South African garnet peridotites recalculated using the Gudmundsson and Wood (1996) oxybarometer

Sample	Locality	P (kbar)	T (°C)	x_{Fa}	x_{Fs}	gt $Fe^{3+}/\Sigma Fe$ (%)	log f_{O_2} (FMQ) (bar)
Luth et al. (1990)							
FRB838	Bultfontein	38	937	0.084	0.075	3.3	–2.9
FRB135	Mothae	38	973	0.069	0.060	5.7	–2.4
PHN1917	Mothae	44	1,075	0.068	0.059	4.8	–3.2
FRB131	Mothae	45	1,081	0.073	0.064	5.4	–2.9
FRB1033	Jagersfontein	56	1328	0.091	0.078	11.6	–2.9
PHN1611	Thaba Putsoa	62	1,452	0.121	0.101	12.2	–3.5
PHN5549	Gibeon Townlands #1	42	1,228	0.088	0.081	5.4	–3.3
PHN1925	Mothae	66	1,453	0.093	0.084	11.8	–3.7
PHN5267	Premier	64	1,415	0.087	0.073	12.1	–3.9
BD2501	Mothae	52	1,298	0.081	0.072	11.2	–2.6
FRB76	Frank Smith	60	1,338	0.088	0.076	11.8	–3.4
FRB140	Mothae	58	1,344	0.093	0.081	10.7	–3.3
Canil and O'Neill (1996)							
BD1140	Bultfontein	40	965	0.082	0.073	5.1	–2.3
BD1150	Bultfontein	49	1,104	0.097	0.083	8.3	–2.5
BD1201	Wesselton	40	981	0.083	0.087	3.3	–3.4
BD1354	Matsoku	60	1,234	0.173	0.147	9.8	–3.7
PHN5239	Finsch	64	1,418	0.085	0.073	10.8	–3.5
PHN5273	Finsch	50	1,231	0.078	0.080	10.6	–2.9
FRB909	Premier	64	1,400	0.091	0.082	11.5	–3.7
FRB921	Premier	39	1,052	0.078	0.070	4.4	–2.8
PHN5267	Premier	64	1,418	0.087	0.073	12.0	–3.9
F865	Premier	52	1,090	0.071	0.061	7.3	–3.3
F556	Premier	59	1,151	0.089	0.072	7.2	–4.0
FRB1350	Premier	21	714	0.083	0.074	3.4	–1.1

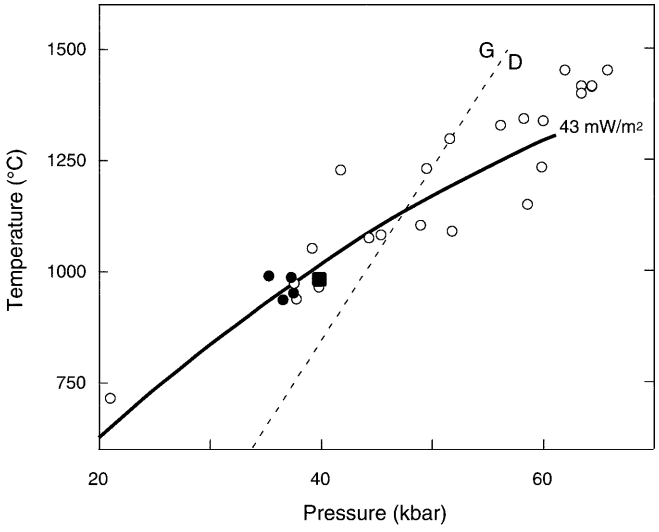

Fig. 4 Pressure–temperature plot for samples from this study (*solid circles*), garnet lherzolite from Wesselton (Carswell and Dawson 1970) (*square*) and garnet peridotites from South Africa (Luth et al. 1990; Canil and O'Neill 1996) (*open circles*). Also shown are *curves* for the graphite–diamond phase boundary (Kennedy and Kennedy 1976) (*dotted line*) and a 43 mW/m^2 model conductive geotherm (Pollack and Chapman 1977) (*solid line*)

(1990) combined with the BK90 garnet–orthopyroxene barometer, or (2) the garnet–olivine thermometer (OW79) combined with the garnet–orthopyroxene barometer (BK90) for assemblages where no clinopyroxene was present. Results from a garnet lherzolite collected from the Wesselton mine (originally described by Carswell and Dawson 1970) gave conditions of 40 kbar and 981 °C, which are nearly identical to the values determined for the metasomatised samples from Wesselton described in the present study.

Oxygen fugacity

Oxygen fugacity was estimated based on the garnet–orthopyroxene–olivine oxybarometer (Luth et al. 1990), which was re-calibrated by Gudmundsson and Wood (1995) using the following reaction:

$$\underset{\text{gt}}{2Fe_3^{2+}Fe_2^{3}\ Si_3O_{12}} \leftrightarrow \underset{\text{ol}}{4Fe_2SiO_4} + \underset{\text{opx}}{2FeSiO_3} + O_2 \quad (1)$$

where $Fe_3{}^{2+}Fe_2{}^{3+}Si_3O_{12}$ is the skiagite component in the garnet. We used the corrected expression for the skiagite activity coefficient reported by Woodland and Peltonen (1999).

Oxygen fugacities corresponding to the different regions of the four garnets are listed in Table 3, where values are given relative to the fayalite–magnetite–quartz (FMQ) buffer of O'Neill (1987) corrected for pressure (Ballhaus et al. 1991). Conditions tend to more oxidising going from core to rim to secondary rim. The calculated relative oxygen fugacities do not vary significantly with temperature or pressure, where a variation of 200 °C or 2 kbar produces a difference in $\Delta\log f_{O2}$ of only 0.2 log-bar units. Therefore, a heating event accompanying metasomatism does not have a significant effect on oxygen fugacities. Uncertainties in the compositions of olivine and orthopyroxene also contribute small errors: ≤ 0.3 log-bar units for a variation in x_{Fe} of ± 0.005. To explain the higher $Fe^{3+}/\Sigma Fe$ values in the secondary rims compared with the cores by changes in temperature or pressure alone would require the secondary rims to have formed below 600 °C, or at pressures more than 47 kbar, and so, in the absence of drastic changes to temperature or pressure during the formation of these garnets, there is a clear indication of an increase in relative oxygen fugacity from core to secondary rim.

Kinetics of oxidation and diffusion

The extent to which differences in oxidation state will be preserved in the garnet depends to varying degrees on (1) the relevant cation and anion diffusion rates in the garnet structure, and (2) the kinetics of the oxidation/reduction reaction. When oxidised fluids infiltrate the mineral assemblage, oxygen in the fluid will react with Fe^{2+} in the garnet to form Fe^{3+}. Oxidation studies of fayalite (Mackwell 1992) and measurements of oxygen self-diffusion in diopside (Farver 1989) indicate that oxygen ions are relatively immobile compared with iron cations, which is probably true for garnet also. The oxidation reaction therefore occurs at the surface of the garnet, and proceeds through diffusion of iron cations through the lattice. The rate of iron diffusion probably provides a minimum estimate for the kinetics of garnet oxidation, based on studies of fayalite oxidation (Mackwell 1992). In upper mantle garnets that are low in Ti, Fe^{2+} occupies only the dodecahedral site, whereas Fe^{3+} occupies only the octahedral site (e.g. Amthauer et al. 1976), implying that exchange of Fe^{2+} and Fe^{3+} in garnet must involve cation exchange over different crystallographic sites, and would be probably of similar magnitude to diffusion rates of other cations in garnet. This would imply that zoning profiles of Fe^{3+} would be preserved on time-scales similar to those of the major and trace elements.

Volume diffusion of iron in garnet is probably controlled by vacancies, hence the diffusivity of cations will vary as a function of oxygen fugacity (e.g. Buening and Buseck 1973). Fe^{2+}/Fe^{3+} diffusivity is probably more sensitive to oxygen fugacity than other major and trace elements, hence increasing oxygen fugacity would increase the rate at which Fe^{2+} is oxidised to Fe^{3+} in the garnet structure. Griffin et al. (1999) noted that the original major and trace element compositions of the garnet cores were probably not preserved, hence it is likely that the original $Fe^{3+}/\Sigma Fe$ of the garnet was also not preserved. The garnet cores therefore reflect a higher

oxygen fugacity than that existing prior to metasomatism.

Implications for diamond preservation

The oxygen fugacities determined from the metasomatised garnet harzburgites of the Wesselton kimberlite can be compared with conditions in other parts of the Kaapvaal craton. We used the values for $Fe^{3+}/\Sigma Fe$ in garnet determined by Luth et al. (1990) and Canil and O'Neill (1996), combined with the chemical analyses reported for coexisting olivine, orthopyroxene and garnet, to calculate the relative oxygen fugacity according to the Gudmundsson and Wood (1995) garnet–orthopyroxene–olivine oxybarometer. Pressures and temperatures were determined as described above. Results show that for nearly all samples, relative oxygen fugacities are lower than those found in the present study (Table 4). In particular, the relative oxygen fugacity calculated for the garnet lherzolite from the Wesselton mine described by Carswell and Dawson (1970) is more than one log-bar unit below the smallest value for the metasomatised assemblage. This is consistent with the conclusion by Griffin et al. (1999) that the garnet cores have also been metasomatised.

The increase in relative oxygen fugacity during metasomatism has some relevance to diamond preservation. The upper oxygen fugacity limit of graphite or diamond stability in harzburgites is defined by the EMOD/EMOG reaction:

$$\underset{\text{opx}}{Mg_2Si_2O_6} + \underset{\text{carbonate}}{2MgCO_3} \leftrightarrow \underset{\text{ol}}{2Mg_2SiO_4} + \underset{\text{dia/gra}}{2C + 2O_2} \quad (2)$$

(Eggler and Baker 1982). Together with the graphite–diamond univariant equilibrium, this defines the maximum stability region of diamond as a function of pressure, temperature and oxygen fugacity in the peridotite system (Fig. 5). The activity of carbonate in the system increases with increasing oxygen fugacity according to reaction (2) until the EMOD boundary is reached. For diamond-bearing assemblages that undergo metasomatism, the degree of diamond preservation is probably influenced by the activity of carbonate in the metasomatic fluid. Increasing carbonate activity would increase the degree of diamond reaction with the fluid, hence causing resorption of the diamond even at oxygen fugacities below the EMOD boundary. Figure 5 illustrates two iso-activity curves for carbonate. Although

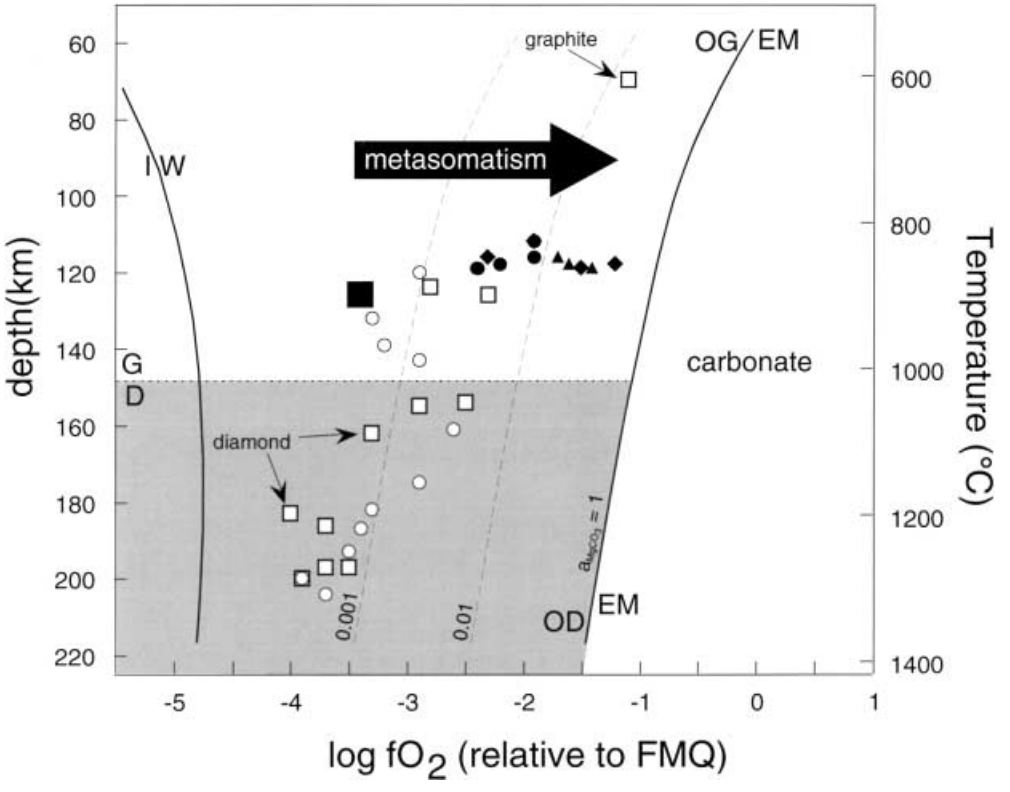

Fig. 5 Oxygen fugacity (relative to FMQ) of garnet peridotites as a function of depth. Zoned garnets from Wesselton (this study) are indicated by *solid circles* (cores), *solid diamonds* (rims) and *solid triangles* (secondary rims), while an unzoned Wesselton sample (Carswell and Dawson 1970; Canil and O'Neill 1996) is indicated by the large solid square. Oxygen fugacities calculated from data of Luth et al. (1990) (*open circles*) and Canil and O'Neill (1996) (*open squares*) are also shown. Assemblages containing graphite and diamond are indicated by *arrows*. The graphite–diamond transition (Kennedy and Kennedy 1976) and the EMOG/EMOD reactions (Eggler and Baker 1982) define the maximum stability region of diamond (*shaded grey*), where *dashed lines* indicate iso-activity curves for carbonate. The iron-wüstite buffer (*P*,*T* formulation of Ballhaus et al. 1991) is indicated for reference, and temperatures are given according to the 43 mW/m^2 model conductive geotherm (Pollack and Chapman 1977)

carbonate activities of 0.001 and 0.01 would not be expected to cause reaction of diamond with the fluid, higher activities could be expected to produce an observable reaction.

The Wesselton mine harzburgites show a progressive oxidation of approximately two log-bar units from the original assemblage to the final stage of metasomatism, nearly reaching the EMOG curve (Fig. 5). This is consistent with suggestions by Griffin et al. (1999) that the fluid in stage (3) was derived from the kimberlite itself, which is generally believed to be a hostile environment to diamonds (Woermann and Rosenhauer 1985 and references therein). Other garnet peridotites from South Africa show significantly lower relative oxygen fugacities, and many lie within the diamond stability field (Fig. 5). Diamond would hence be preserved during the initial stages of metasomatism, up to an increase in relative oxygen fugacity of 1–2 log-bar units. Beyond that point, however, the fluid would react with the diamonds, leading to their oxidation and resorption.

Acknowledgements The work benefited from helpful discussions with S. Chakraborty and A.B. Woodland, and was improved through reviews by Dante Canil and an anonymous reviewer. S.R. Shee thanks the management of Stockdale Prospecting Limited and De Beers Exploration for permission to publish this paper. This is publication no. 233 from the ARC National Key Centre for Geochemical Evolution and Metallogeny of Continents.

References

Amthauer G, Annersten H, Hafner SS (1976) The Mössbauer spectrum of ^{57}Fe in silicate garnets. Z Krist 143:14–55

Angel RJ, McCammon CA, Woodland AB (1998) Structure, ordering and cation interactions in Ca-free $P2_1/c$ clinopyroxenes. Phys Chem Mineral 25:249–258

Ballhaus C, Berry RF, Green DH (1991) High pressure experimental calibration of the olivine–orthopyroxene–spinel oxygen barometer: implications for the oxidation state of the upper mantle. Contrib Mineral Petrol 107:27–40

Brey GP, Köhler T (1990) Geothermobarometry in four-phase lherzolites. II. New thermobarometers, and practical assessment of existing thermobarometers. J Petrol 31:1353–1378

Buening DK, Buseck PR (1973) Fe–Mg lattice diffusion in olivine. J Geophys Res 78:6852–6862

Canil D (1999) The Ni-in-garnet geothermometer: calibration at natural abundances. Contrib Mineral Petrol 136:240–246

Canil D, O'Neill HStC (1996) Distribution of ferric iron in some upper-mantle assemblages. J Petrol 37:609–635

Carswell DA, Dawson JB (1970) Garnet pridotite xenoliths in South African kimberlite pipes and their petrogenesis. Contrib Mineral Petrol 25:163–184

De Grave E, Van Alboom A (1991) Evaluation of ferrous and ferric Mössbauer fractions. Phys Chem Mineral 18:337–342

Eggler DH, Baker DR (1982) Reduced volatiles in the system C–O–H: implications to mantle melting, fluid formation, and diamond genesis. In: Akimoto S, Manghnani MH (eds) High pressure research in geophysics. Center for Academic Publications Japan, Tokyo, pp 237–250

Farver JR (1989) Oxygen self-diffusion in diopside with application to cooling rate determinations. Earth Planet Sci Lett 92:386–396

Geiger CA, Armbruster T, Lager GA, Jiang GA, Lottermoser W, Amthauer G (1992) A combined temperature dependent ^{57}Fe Mössbauer and single crystal X-ray diffraction study of synthetic almandine: evidence for the Gol'danskii–Karagin effect. Phys Chem Mineral 19:121–126

Gibb TC (1978) The orientation of the electric-field-gradient tensor from single-crystal Mössbauer measurements. J Chem Soc Dalton Trans, pp 743–752

Griffin WL, Cousens DR, Ryan CG, Sie SH, Suter GF (1989) Ni in chrome pyrope garnets: a new geothermometer. Contrib Mineral Petrol 103:199–202

Griffin WL, Shee SR, Ryan CG, Win TT, Wyatt BA (1999) Harzburgite to lherzolite and back again: metasomatic processes in ultramafic xenoliths from the Wesselton kimberlite, Kimberly, South Africa. Contrib Mineral Petrol 1999:232–250

Gudmundsson G, Wood BJ (1995) Experimental tests of garnet peridotite oxygen barometry. Contrib Mineral Petrol 1995:56–67

Harley SL (1984a) An experimental study of the partitioning of Fe and Mg between garnet and orthopyroxene. Contrib Mineral Petrol 86:359–373

Harley SL (1984b) The solubility of alumina in orthopyroxene coexisting with garnet in $FeO–MgO–Al_2O_3–SiO_2$ and $CaO–FeO–MgO–Al_2O_3–SiO_2$. J Petrol 25:665–696

Kennedy CS, Kennedy GC (1976) The equilibrium boundary between graphite and diamond. J Geophys Res 81:2467–2470

Luth RW, Canil D (1993) Ferric iron in mantle-derived pyroxenes and a new oxybarometer for the mantle. Contrib Mineral Petrol 113:236–248

Luth RW, Virgo D, Boyd FR, Wood BJ (1990) Ferric iron in mantle-derived garnets. Implications for thermobarometry and for the oxidation state of the mantle. Contrib Mineral Petrol 104:56–72

Lyubutin IS, Dodokin AP (1971) Temperature dependence of the Mössbauer effect for Fe^{2+} in dodecahedral coordination in garnet. Sov Phys Crystallogr 15:1091–1092

Lyubutin IS, Dodokin AP, Belyaev LM (1970) Temperature dependence of the Mössbauer effect for octahedral iron atoms in garnet. Sov Phys – Solid State 12:1100–1102

Mackwell SJ (1992) Oxidation kinetics of fayalite (Fe_2SiO_4). Phys Chem Mineral 19:220–228

McCammon CA (1994) A Mössbauer milliprobe: practical considerations. Hyper Int 92:1235–1239

McCammon (1999) Methods for determination of $Fe^{3+}/\Sigma Fe$ in microscopic samples. In: Gurney JJ, Gurney JL, Pascoe MD, Richardson SH (eds) The PH Nixon Volume, Proc VII Int Kimberlite Conf, vol 2. Red Roof Design, Cape Town, South Africa, pp 540–544

McCammon CA, Chaskar V, Richards GG (1991) A technique for spatially resolved Mössbauer spectroscopy applied to quenched metallurgical slags. Measure Sci Technol 2:657–662

McCammon CA, Griffin WL, Shee SH, O'Neill HSC (1995) Determination of ferric iron variation within zoned garnets from the Wesselton kimberlite using a Mössbauer milliprobe. In: 6th Int Kimb Conf Ext Abstr, pp 362–364

O'Neill HSC (1980) An experimental study of Fe–Mg partitioning between garnet and olivine and its calibration as a geothermometer: corrections. Contrib Mineral Petrol 72:337

O'Neill HSC (1987) Quartz–fayalite–iron and quartz–fayalite–magnetite equilibria and the free energy of formation of fayalite (Fe_2SiO_4) and magnetite (Fe_3O_4). Am Mineral 72:67–75

O'Neill HSC, Wood BJ (1979) An experimental study of Fe–Mg partitioning between garnet and olivine and its calibration as a geothermometer. Contrib Mineral Petrol 70:59–70

Osborne MD, Fleet ME, Bancroft GM (1981) $Fe^{2+}–Fe^{3+}$ ordering in chromite and Cr-bearing spinels. Contrib Mineral Petrol 77:251–255

Pollack HN, Chapman DS (1977) On the regional variation of heat flow, geotherms, and lithospheric thickness. Tectonophysics 38:279–296

Rancourt DG, McDonald AM, Lalonde AE, Ping JY (1993) Mössbauer absorber thicknesses for accurate site populations in Fe-bearing minerals. Am Mineral 78:1–7

Rancourt DG, Christie IAD, Royer M, Kodama H, Robert J-L, Lalonde AE, Murad E (1994) Determination of accurate $^{[4]}Fe^{3+}$, $^{[6]}Fe^{3+}$, and $^{[6]}Fe^{2+}$ site populations in synthetic annite by Mössbauer spectroscopy. Am Mineral 79:51–62

Ryan CG, Griffin WL, Pearson NJ (1996) Garnet geotherms: Pressure–temperature data from Cr-pyrope garnet xenocrysts in volcanic rocks. J Geophys Res 101:5611–5625

Shinno I (1981) A Mössbauer study of ferric iron in olivine. Phys Chem Mineral 7:91–95

Sobolev VN, McCammon CA, Taylor LA, Snyder GA, Sobolev NV (1999) Precise Mössbauer milliprobe determination of ferric iron in rock-forming minerals and limitations of electron microprobe analysis. Am Mineral 84:78–85

Woermann E, Rosenhauer M (1985) Fluid phases and the redox state of the Earth's mantle. Fortschr Mineral 63:263–349

Woodland AB, Peltonen P (1999) Ferric iron contents of garnet and clinopyroxene and estimated oxygen fugacities of peridotite xenoliths from the Eastern Finland Kimberlite Province. In: Gurney JJ, Gurney JL, Pascoe MD, Richardson SH (eds) The PH Nixon Volume, Proc VII Int Kimberlite Conf,. Red Roof Design, Cape Town, South Africa, pp 904–911